Food Hydrocolloids 134 (2023) 108031

Contents lists available at ScienceDirect

Food Hydrocolloids

journal homepage: www.elsevier.com/locate/foodhyd

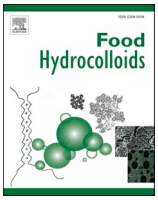

Effects of kappa-carrageenan on egg white ovalbumin for enhancing the gelation and rheological properties via electrostatic interactions

Yuzhu Mao [a], Min Huang [b], Jiapei Bi [a], Duowen Sun [a], Hongliang Li [d], Hongshun Yang [a,c,*]

[a] Department of Food Science and Technology, National University of Singapore, 117542, Singapore
[b] School of Food Science and Biotechnology, Zhejiang Gongshang University, Hangzhou, 310018, PR China
[c] National University of Singapore (Suzhou) Research Institute, 377 Lin Quan Street, Suzhou Industrial Park, Suzhou, Jiangsu, 215123, PR China
[d] Guangzhou Welbon Biological Technology Co., Ltd, Guangzhou, Guangdong, 523660, PR China

ARTICLE INFO

Keywords:
Egg protein
Polysaccharide
Rheology
Confocal laser scanning microscope (CLSM)
Fourier transform infrared spectroscopy (FTIR)

ABSTRACT

The protein-polysaccharide system is natural, and it has been widely applied in food manufacturing in recent years. However, the interactions in the system might be affected by numerous factors and this research investigated the effects of κ-carrageenan (κ-C) on the structure, interaction, and rheological characteristics of egg white ovalbumin (OVA) before and after heating. The zeta potential was adopted to show the surface charge of mixtures and its combination with turbidity test was used to discover the maximum associative interaction at the critical mixing ratio of κ-C: OVA. The results evidenced that the electrostatic interaction formed between OVA and κ-C. The critical ratio of OVA: κ-C (w/w) at 92:8 showed the minimum net charge (-0.5 ± 0.3 mV) and the maximum turbidity (0.122 ± 0.001 cm^{-1}). All κ-C/OVA mixtures were observed shear thinning behaviour. The mixtures at 92:8 performed the highest apparent viscosity (η) and remained the maximum complex modulus (G^*) in the thermal cycle. The κ-C/OVA complex network was observed stronger than pure κ-C or OVA through the confocal scanning laser microscopy (CLSM). The rheological properties of the 92:8 mixtures supported the strongest electrostatic interactions between κ-C and OVA, corresponding to the largest aggregates structure in the CLSM images. A schematic model was further verified at the secondary structure of OVA using Fourier transform infrared (FTIR) spectroscopy. This study provides instructions to design innovative food systems that contain κ-C and OVA.

1. Introduction

In the multi-component food systems, two main kinds of biopolymers, protein and polysaccharide, and mixtures of them are widely used in the food industry. Polysaccharides and proteins are natural food macromolecules, which present thickening, gelating and texturing properties (Gentile, 2020; Ye, 2008). Protein-polysaccharide interactions contribute to the structure, stability, texture and mouthfeel of food. Meanwhile, the food industry often adopts heat treatment to destroy microbial pollution or low pH to prevent microbial growth (Campbell, Raikos, & Euston, 2003). When pH is lower than the isoelectric point (pI) of protein, it contains positive charged (Lu et al., 2020). When the protein and polysaccharide are oppositely charged at the low pH, the coacervation formed at the critical pH (pH_c) (Gentile, 2020). The complex coacervates have the potential to be utilized as novel biomaterials, due to their excellent bioactivity, biosafety and biocompatibility (Lu et al., 2020).

Egg white has been widely used as an ingredient in food systems such as baking food as a good protein resource. Considering the components, egg white contains numerous types of protein, such as ovalbumin (OVA), conalbumin, ovomucoid, ovomucin, and lysozyme (Abeyrathne, Lee, & Ahn, 2013). Among them, OVA occupies 54% of the total egg white protein (Abeyrathne et al., 2013). The high quantity of ovalbumin corresponds with its powerful effects on the functionality of egg white. Therefore, OVA is often adopted as a model protein when exploring egg white protein (Xiong & Ma, 2017). OVA is a kind of protein containing free sulfhydryl groups with a molecular weight of 44.5 kDa (Mine, 1995). As a single peptide chain, it contains 385 amino acids and more than 50% of them are hydrophobic, which provide the emulsion and foaming capacity for the egg white to meet the complex needs of food manufacturing, such as baking products, meringues, meat products, and cookies (Mine, 1995; Zhao et al., 2016).

* Corresponding author. Department of Food Science & Technology, National University of Singapore, Science Drive 2, 117542, Singapore.
E-mail address: fstynghs@nus.edu.sg (H. Yang).

https://doi.org/10.1016/j.foodhyd.2022.108031
Received 12 April 2022; Received in revised form 17 July 2022; Accepted 29 July 2022
Available online 5 August 2022
0268-005X/

Carrageenan is a group of hydrophilic linear sulphated polysaccharides extracted from marine edible red algae (Necas & Bartosikova, 2013). It has been proved to have numerous health-functional properties, such as antioxidant, immunomodulatory activities, and prebiotic effects (Kobayashi, Kumagai, Yamamoto, Yasui, & Kishimura, 2020; Necas & Bartosikova, 2013). Kappa-carrageenan (κ-C) has only one ester sulphate group per disaccharide repeating unit, which leads to a higher gel strength for κ-C (Du, Brenner, Xie, & Matsukawa, 2016). In solution, the gelation process of κ-C has two stages: the random coil-to-helix transition and a space-spanning network formed by the helices aggregate introducing positive ions (Takemasa, Chiba, & Date, 2001). Meanwhile, κ-C has the thermo-reversible characteristic and has been widely applied as a thickening, stabiliser, and texturing agent in the food industry (Mangione, Giacomazza, Bulone, Martorana, & San Biagio, 2003; Tan & Joyner, 2018).

The addition of polysaccharides was reported to efficiently improve the emulsifying stability and gelling property of OVA in different processing conditions (Chen et al., 2018). The OVA/κ-C system exists in food commonly and this low-cost, native, and safe system has been applied widely as fish cryoprotectant and the carriers of bio-components (Walayat et al., 2021; Xie et al., 2019). In addition, the OVA/κ-C system can form edible films, fat replacers, and novel semi-solid food products, and has a great potential for developing new novel systems (Le, Rioux, & Turgeon, 2017). Although there are several studies about the OVA and κ-C system, little information about the physicochemical properties of OVA/κ-C coacervation and the characteristics of the mixing ratio of κ-C: OVA at pH_c is not clear. Therefore, to know better about the interaction between OVA and κ-C, further research is needed to promote the application of the OVA/κ-C system.

The main goal of this study was to understand the effects of κ-C on the physicochemical characteristics of OVA after the application of thermal treatment. In order to achieve this goal, the zeta potential was adopted to reveal the surface charge of samples and it was used to find out the maximum associative interaction at a critical mixing ratio of κ-C: OVA. The apparent viscosity and thermal gelation process of the OVA/κ-C mixtures were evaluated by a rheometer. The morphology of mixtures structure was investigated through the confocal laser scanning microscope (CLSM). Finally, the mechanism for the changes of the secondary structure of OVA was validated by Fourier transform infrared (FTIR) spectroscopy analysis. The results can help to further understand the interactions between OVA and κ-C and promote the development of related food systems.

2. Materials and methods

2.1. Materials and sample preparation

The OVA (ovalbumin, ≥ 98%) and κ-C (kappa-carrageenan) were gained from Sigma Aldrich (Singapore). Rhodamine B, fluorescein isothiocyanate (FITC), HCl, and ethanol were purchased from Merck (Darmstadt, Germany). All the other chemical reagents adopted were in analytical grade and from Sigma Aldrich (Singapore).

The OVA and κ-C powder were accurately weighed, separately dissolved in deionised water, and stirred at 300 r/min for 30 min at room temperature to prepare the OVA solution (1.0%, w/w) and the κ-C solution (0.5%, w/w), respectively. The pH values were adjusted to 3.0 ± 0.1 through 1 mol/L HCL. In the unheated sample, OVA solutions were mixed with the κ-C solution at different ratios (90:10, 92:8, 94:6, 96:4, 98:2, w/w) by stirring at 700 r/min for 1.5 h (Xie et al., 2019). In the heated samples, the unheated sample (5 mL) was heated to 90 °C for 30 min and then cooled down to room temperature.

2.2. Zeta potential measurement

Zeta potential measurement for all OVA/κ-C samples was assessed through a NanoBrook Omni Zeta potential analyser (Brookhaven Instruments, NY, USA) (Sow, Chong, Liao, & Yang, 2018). The OVA/κ-C unheated samples were diluted to 0.01% (w/w) with DI water, followed by stirring for 1 h at room temperature. The phase analysis light scattering (PALS) model was adopted.

2.3. Turbidity

The turbidity of the OVA/κ-C mixtures dilutions (20-fold dilution) was evaluated with an ultraviolet–visible spectrophotometer (UV-2600, Shimadzu, Japan) to obtain the optical density at the UV wavelength of 600 nm at 25 °C (Sow, Toh, Wong, & Yang, 2019). Turbidity (T, cm^{-1}) was calculated by the following equation:

$$T = -(1/L)In(I/I_0)$$

where L represents the optical range length of 1 cm, I and I_0 represent the intensity of the sample and the blank, respectively. DI-water was used as the blank.

2.4. Rheological tests

Rheological analyses were conducted through a stress-controlled rheometer (MCR 102, Anton Paar, Graz, Austria) equipped with a cone-and-plate geometry with a diameter of 60 mm, a cone angle of 1° and a fixed gap of 0.116 mm. The excess sample was removed and coated with silicone oil to avoid water evaporation (Njintang et al., 2006).

2.4.1. Viscosity measurement

The linear viscoelastic region (LVR) of the sample was determined by the strain sweep test in the range of 0.01–100% with a frequency fixing at 1 Hz (Huang, Mao, Li, & Yang, 2021). The steady shear flow measurement of all samples was presented at 20 °C with the operating shear rate ranging from 0.01 to 10 s^{-1}. The experimental data could be described by the power-law equation as follow:

$$\eta = K \cdot \dot{\gamma}^{n-1} \quad \text{Eq (1)}$$

where η is apparent viscosity (Pa•s), K is consistency coefficient (Pa•s^n), $\dot{\gamma}$ is the shear rate (s^{-1}), and n is the flow behaviour index.

2.4.2. Temperature ramp test

The temperature sweep was performed from 20 to 90 °C, kept at 90 °C for 30 min, and then decreased from 90 °C to 20 °C (rate = 1.5 °C/min) (Huang et al., 2021).

2.5. Confocal laser scanning microscope (CLSM) analysis

The microstructure of OVA/κ-C complexes was analysed by CLSM (Olympus, FV1000, Tokyo, Japan) (Huang et al., 2021; Sow et al., 2018). Rhodamine B and FITC (0.1 g/L in ethanol, with the ratio of 1:1.5, v/v) were used to label OVA and κ-C, respectively (Liu, Maruyama, Masuda, Honda, & Arai, 2014). In a dim environment, the dye mixture was added to the samples at the ratio of 1:100 (dye: samples, w/w). The excitation/emission wavelengths of the rhodamine B and FITC were 540/625 nm and 490/525 nm, respectively. Microscopic images of the stained sample solutions before and after heating were taken at a 10 × immersion magnification.

2.6. FTIR spectroscopy analysis

All samples were freeze-dried and mixed with KBr powder by milling (1 mg sample/50 mg KBr) to prepare the pellet. The KBr powder was dried around 100 °C for 24 h and the milling process was completed under an infrared light to reduce water error. The samples were scanned 64 times in the range of 4000–450 cm^{-1} with a resolution of 4 cm^{-1} using the FTIR spectrometer (PerkinElmer, Waltham, MA, USA). The

spectra of the samples were pre-processed for background removal, baseline correction, and normalization using the spectroscopy software. The amide I (1600-1700 cm^{-1}) was self-deconvoluted and further studied. It was performed with a bandwidth of around 20 and an enhancement factor of 1.5 through Omnic 8.2 (Thermo Fisher Scientific Inc. Waltham, MA, 260 U.S.A). The deconvoluted spectra were fitted with OriginPro 9.0 software (OriginLab, Northampton, MA, USA) and the Gaussian curve fitting function (Determan, Graham, Pfeiffer, & Narasimhan, 2006; Ngarize, Herman, Adams, & Howell, 2004).

2.7. Statistical analyses

All analyses were conducted in triplicates independently and the results were described as the mean and standard derivation. ANOVA with a Student-Newman-Keuls (SNK) was performed with SPSS (IBM Corp., Armonk NY USA) with $P < 0.05$ being regarded as statistically significant.

3. Results and discussion

3.1. Zeta potential and turbidity of OVA/κ-C mixtures

Zeta potential, which relates to the stability of the colloidal dispersion, is a vital index for colloidal systems. The electrostatic potential can reflect the change of ovalbumin conformation (Gonzalez-Perez, Ruso, Prieto, & Sarmiento, 2004). The zeta potential values of different OVA/κ-C systems are shown in Fig. 1A. The zeta potential of κ-C was −31.36 mV because it had the negatively charged sulphate group (Spagnuolo, Dalgleish, Goff, & Morris, 2005). Conversely, the zeta potential value of pure OVA was 11.14 mV at pH 3.0. The isoelectric point (pl) of OVA is 4.5, the particle charge of the OVA solution was positive due to the protonation of the amino acid residues at pH 3.0 (Kang, Ryu, Park, Czarnik-Matusewicz, & Jung, 2014). The addition of κ-C influenced the zeta potential values of OVA/κ-C systems significantly (Fig. 1A). The zeta potential values of 92:8 and 94:6 samples were −0.50 mV and −2.24 mV, respectively. The value was quite closer to neutral, indicating that the positively charged OVA and negatively charged κ-C in the systems tended to achieve balance. The electrostatic interactions can form between the sulphate group ($-OSO_3^-$) of κ-C and the amino group ($-NH_3^+$) of OVA (Lu et al., 2020). Since the OVA and κ-C were oppositely charged at pH 3.0, the protein-polysaccharide interactions might occur and form OVA-κ-C complexes (Gentile, 2020).

The effects of the κ-C addition on the turbidity of mixtures are shown in Fig. 1B. The turbidity changes of samples were the indication of coacervation resulting from electrostatic attraction of oppositely charged protein and polysaccharide (Gentile, 2020; Sow et al., 2019). All the OVA/κ-C mixtures showed significantly higher turbidity when compared with the pure OVA (0.003 cm^{-1}) and κ-C solutions (0.019 cm^{-1}), illustrating that the insoluble complexes were formed in the OVA/κ-C mixtures. The turbidity achieved the maximum of 0.122 cm^{-1} at the ratio of 92:8, which might be attributed to the almost neutral charge of the OVA/κ-C system (Fig. 1A). As the increase of κ-C concentration, the turbidity of samples decreased but had no significant difference (samples at the ratio of 94:6, 96:4, and 98:2). The relatively higher net charge in these systems led to the repulsion between the molecules (Wijaya, Patel, Setiowati, & Van der Meeren, 2017). This repulsion may prevent the formation of coacervation and result in the decrease of turbidity.

Based on the zeta potential and turbidity results, it was obvious that the mixing ratio was an important factor for the insoluble complex formation. The charge of OVA/κ-C mixtures was close to neutralizated and the turbidity reached the maximum at the ratio of 92:8, indicating that the ratio of 92:8 was the critical mixing ratio.

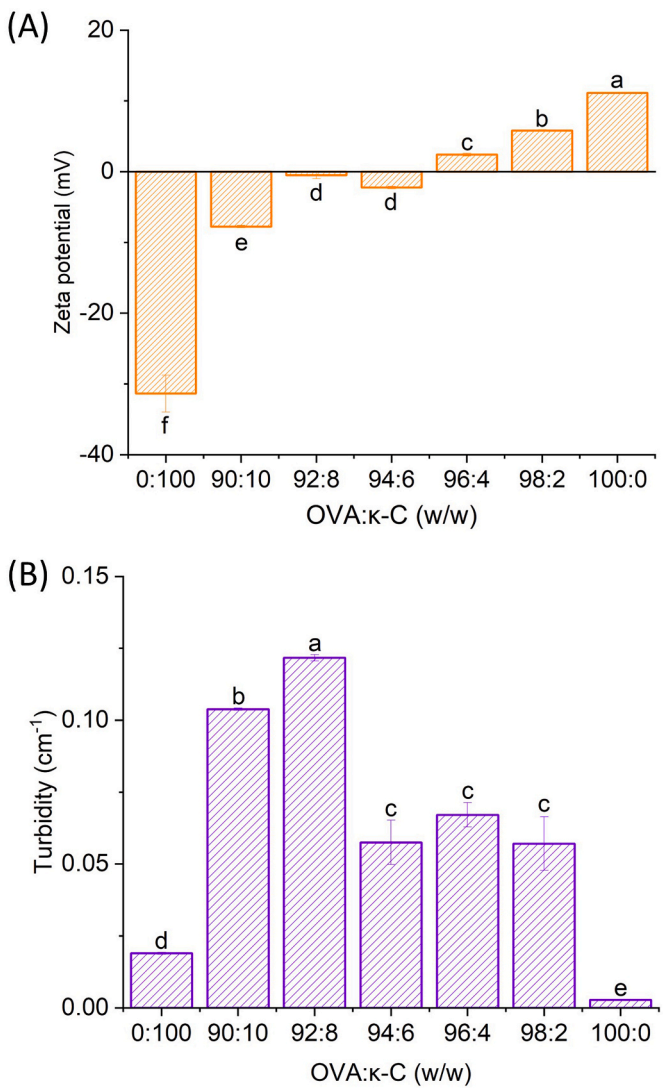

Fig. 1. Effects of different mixing ratios of kappa-carrageenan (κ-C) and ovalbumin (OVA) mixtures on zeta potential (A) and turbidity (B). Values are expressed as mean with standard deviation. Values with different letters differ significantly at $P < 0.05$ (n = 3).

3.2. Viscosity of different OVA/κ-C mixtures

The apparent viscosity as a function of shear rate of the OVA/κ-C samples is shown in Fig. 2A. It was observed that the apparent viscosity declined with the increase of the shear rate, indicating that all OVA/κ-C mixtures showed shear thinning behaviour. Similar results have been reported in the OVA/gum arabic-stabilized emulsion (Niu et al., 2016). Both pure OVA and κ-C samples exhibited relatively low apparent viscosity. The apparent viscosity of OVA/κ-C mixtures reached the highest value at the ratio of 92:8. Based on the results of zeta potential and turbidity, the charge of OVA/κ-C mixtures was close to neutralizated and the turbidity reached the maximum at the ratio of 92:8. Thus, the increased values of apparent viscosity may be related to the formation of the insoluble complexes (Souza & Garcia-Rojas, 2017). The apparent viscosity of protein/polysaccharide coacervates was proved to be determined by the electrostatic interactions rather than the viscosity of biopolymers (Niu et al., 2018). At the ratio of 92:8, the surface charges were close to neutral and had stronger electrostatic interactions between OVA and κ-C than other complexes. The higher apparent viscosity related to the easier formation of aggregates when stronger electrostatic interactions existed. In the other systems, the polysaccharides or OVA

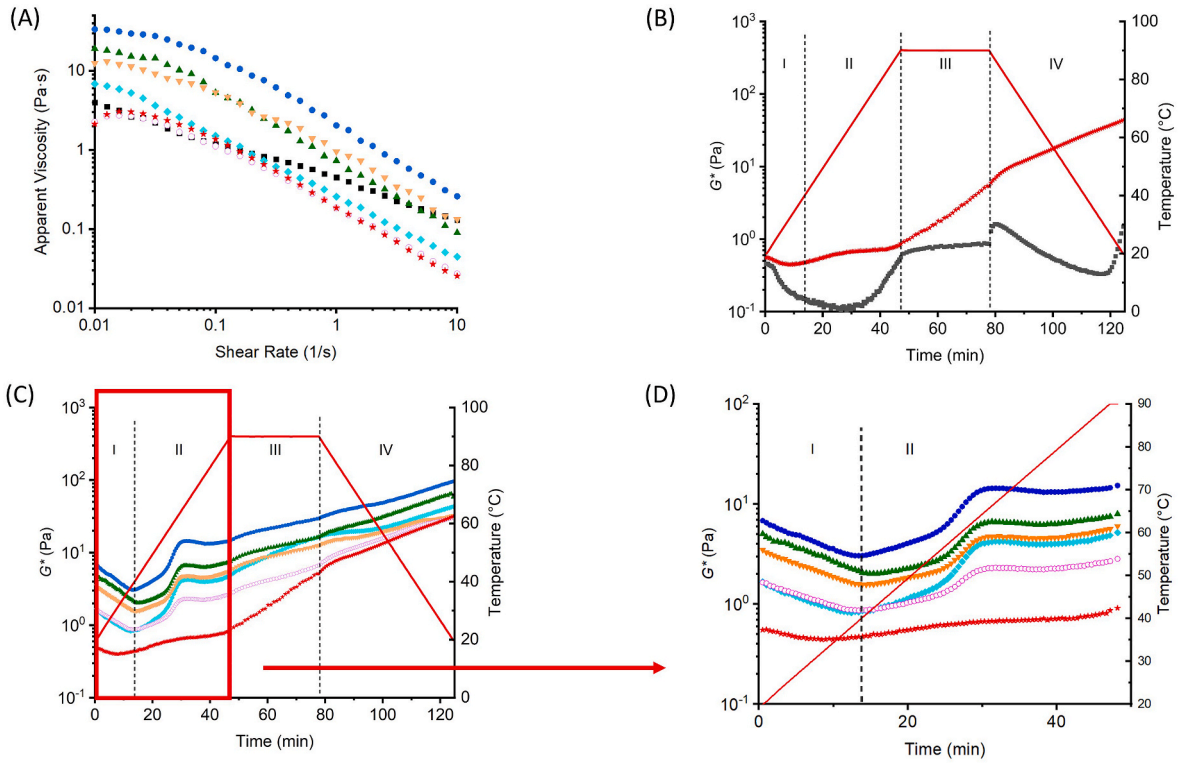

Fig. 2. The flow curve about shear rate-apparent viscosity of the different OVA/κ-C mixtures (A); The evolution of the complex modulus (G^*) of OVA solution (1.0 %, w/w) and the κ-C solution (0.5%, w/w) (B); The G^* of different OVA/κ-C complexes during the whole thermal cycle (C) and during the heating period (zoomed in the phase I & II) (D).
OVA: κ-C: ■, 0:100; ◆, 90:10; ●, 92:8; ▲, 94:6; ▼, 96:4; ○, 98:2; ★, 100:0.

were excessed. The electrostatic repulsion between extra negatively charged κ-C or the excessed positively charged OVA repelled with each other, resulting in a more stable system (Gentile, 2020). Thus, the extra charge can inhibit the formation of the insoluble complexes, resulting in lower apparent viscosity.

The power-law model has been widely utilized in fluid food systems (Huang et al., 2021). As shown in Table 1, except for mixtures at the critical mixing ratio (98:2), the K values of other OVA/κ-C mixtures showed no significant changes compared with pure OVA and κ-C. Only at the critical ratio of 92:8, the K value (1.950 ± 0.528) was significantly higher than those of the other samples, which was consistent with the apparent viscosity values. It showed the increase of consistency of the mixtures, presenting apparent viscosity more relying on shear rate (Huang et al., 2021). The rheological behaviour of complexes between protein and polysaccharide is generally shear thinning (Schmitt & Turgeon, 2011). Here in this study, the flow behaviour index n was in the range of 0.117–0.501, which also indicated that the samples showed shear-thinning behaviour. Compared with the OVA solution, the n values of OVA/κ-C systems did not change significantly, meaning that the addition of κ-C in low concentration had no significant influence on the flow behaviour of the mixtures.

Table 1
Power-law model constants for the OVA/κ-C mixtures at different mixing ratios.

OVA: κ-C (w/w)	K (Pa·s^n)	n	R^2	RMSE
0:100	0.410 ± 0.040^b	0.581 ± 0.047^a	0.921	0.055
90:10	0.254 ± 0.089^b	0.234 ± 0.019^b	0.997	0.176
92:8	1.950 ± 0.528^a	0.235 ± 0.052^b	0.974	2.164
94:6	0.704 ± 0.202^b	0.166 ± 0.043^b	0.985	1.019
96:4	0.861 ± 0.188^b	0.301 ± 0.090^b	0.967	0.592
98:2	0.178 ± 0.007^b	0.287 ± 0.013^b	0.979	0.223
100:0	0.180 ± 0.063^b	0.264 ± 0.034^b	0.968	0.320

* Values are expressed as mean ± standard deviation. Values with different letters in the same column differ significantly at $P < 0.05$ (n = 3).

3.3. The thermal gelation process of different OVA/κ-C mixtures

The complex modulus (G^*) values of the OVA and κ-C solutions during the thermal cycle are shown in Fig. 2B. During the whole thermal cycle, the pure κ-C solution was at quite low viscoelastic values in the whole analysis compared with the OVA solution. At the end of the thermal cycle, the slight increase of the G^* value was caused by the formation of κ-C gels after cooling. The κ-C can form the thermo-reversible gel and involves in the conformational change during the thermal cycle (Mangione et al., 2003). The same phenomenon was also gained in a previous study about the thermal gelation of yolk/κ-C systems (Huang et al., 2021).

The thermal behaviour of the globular protein and carrageenan gelation can be divided into four regions. Region I: Slightly decrease can be observed in G^* values, which caused by the heat-induced mobility of mixtures and no protein denaturation occurred. Region II: The G^* value increased because thermal stimulated the OVA/κ-C interaction, the mixtures may undergo conformational changes. Region III: A slight increase of the G^* value was observed, the OVA/κ-C complexes association formed the gelation. Region IV: During the cooling phase, the samples showed a sharp increase in the G^* values and formed a stronger gel network. These regions were also certified in previous analyses (Huang et al., 2021; Sánchez-Gimeno, Vercet, & López-Buesa, 2006).

For the pure OVA sample, the low G^* values were kept in region I and II, indicating that the heat treatment had few effects on the viscoelastic properties in this period (Fig. 2B). When the temperature reached over 80 °C, a slight increase of the G^* value was observed. Since the denaturation temperature of OVA is 72 °C, the higher gel strength resulted from the denaturation of the OVA (Niu et al., 2016). During the cooling

phase, the OVA sample showed a rapid increase in the G^* value corresponds with stronger gel network, due to the hydrogen bonds formed between the protein chains (Mine, 1995).

Since the concentration of OVA is rather higher than that of carrageenan in the mixtures, all samples showed similar protein gelation in the thermal process and combine with the polysaccharide gelation (Sánchez-Gimeno et al., 2006). The whole temperature rise period (region I, II) was shown in Fig. 2C and D, the G^* value slightly decreased in the first region. The increase of heat stimulated the mixtures mobility, thus OVA/κ-C complexes might be partially destroyed (Huang et al., 2021). In the second region, the G^* value increased sharply with addition κ-C in the mixtures and reached the highest value at the critical mixing ratio of 98:2. The protein proved to combine with oppositely charged polysaccharides to form coacervation (Gentile, 2020). The protein-polysaccharide complex is a kind of molecules rearrangements and the mixtures had a better-organised crystal structure (Niu et al., 2016). Due to the balanced zeta potential in the system of 92:8, the OVA/κ-C mixtures might form a well-organised structure with higher viscoelasticity. During the period before the third region (about 30–50 min), the G^* value of all mixture samples slight decreased. It may be because the protein-polysaccharide interaction in the OVA/κ-C coacervation inhibited the aggregation of OVA in the system (Huang et al., 2021). The interactions between protein-protein were weak and may be destroyed under heat treatment. This phenomenon was also observed in the OVA/dextran sulphate system (Liu et al., 2021).

As shown in Fig. 2C, during the third region, it is obvious that the increase of G^* value in the mixtures was higher than the sum of G^* of κ-C and OVA individually. Therefore, the increasing G^* might be attributed to the aggregation of the negative charges of sulphate groups in the κ-C and the positively charged groups of the unfolded OVA, leading to the formation of the stronger gel network (Sánchez-Gimeno et al., 2006). Thus, the G^* value of the sample at 92:8 was the highest, because the excess charged groups in other mixtures may weaken inhibit the aggregation of the complexes. In the fourth region, the G^* value steeply increased as the temperature decreased. The increased G^* was probably caused by the enhanced interconnection of the OVA-κ-C complexes. At the end of the cooling phase, the sample of 92:8 showed much higher G^* value than the sample containing only OVA. This phenomenon might be based on the rearrangement of the protein/polysaccharide structures after complex formation, and OVA might hide in the κ-C chains, or the re-organised network formation (Lam, Paulsen, & Corredig, 2008; Niu et al., 2018). Overall, the addition of κ-C significantly increased the viscoelastic properties of OVA during the whole thermal test.

3.4. Confocal laser scanning microscope (CLSM) analysis of OVA/κ-C mixtures

The morphology images of OVA, κ-C solution and OVA/κ-C mixtures before and after heating are shown in Figs. 3 and 4. The κ-C was green as the polysaccharide with FITC and the OVA was red as the protein with Rhodamine B (Huang et al., 2021). The numerous green dots in κ-C and the green area in all mixtures should be the κ-C. The spherical aggregates in red should be the OVA because the ovalbumin is a globular protein (Clark, Kavanagh, & Ross-Murphy, 2001).

Before the heating treatment, the addition of κ-C was associated with the formation of insoluble complexes, and the mixing ratios of OVA/κ-C systems had considerable influences on the size of the aggregations (Fig. 3). The insoluble protein-polysaccharide coacervation was established by the electrostatic binding of protein (cationic) and polysaccharide (anionic) (Gentile, 2020). The formation of protein-polysaccharide coacervation companied the rearrangement of structure (Niu et al., 2018). Owing to the small molecular weight of OVA, part of the OVA molecules was buried in the linear κ-C polysaccharide and formed loosely structured aggregations. This was similar to the structure of milk protein/pullulan (Wang, Van Dijk, Odijk, & Smit, 2001). At the critical mixing ratio at 92:8, the largest aggregates formed in the samples (Fig. 3C). This may be because the zeta potential value of the mixture was close to neutral. It indicated that the electrostatic gravitational force of the positively charged OVA to the negatively charged κ-C was neutralized. As the OVA or κ-C ratio increased, the size of the aggregations reduced, verifying that the excess net charge interferes with the formation of complexes.

Mixing ratios also significantly affect the structure of OVA/κ-C complexes after heating (Fig. 4). The OVA aggregation can be observed due to the denaturation of the protein leading to the exposure of the hydrophobic group (Mine, 1995). The size of OVA/κ-C complexes became small after heating. At the mixing ratio of 90:10, only partial κ-C forms complexes with OVA and the OVA aggregates still dominated the system (Fig. 4I). It may be because the excess negative charge of the κ-C affected the formation of the reorganized structure during heating. At the mixing ratio of 92:8 and 94:6, the mixtures had a larger size than other samples (Fig. 4J and K). Due to the charge was close to the

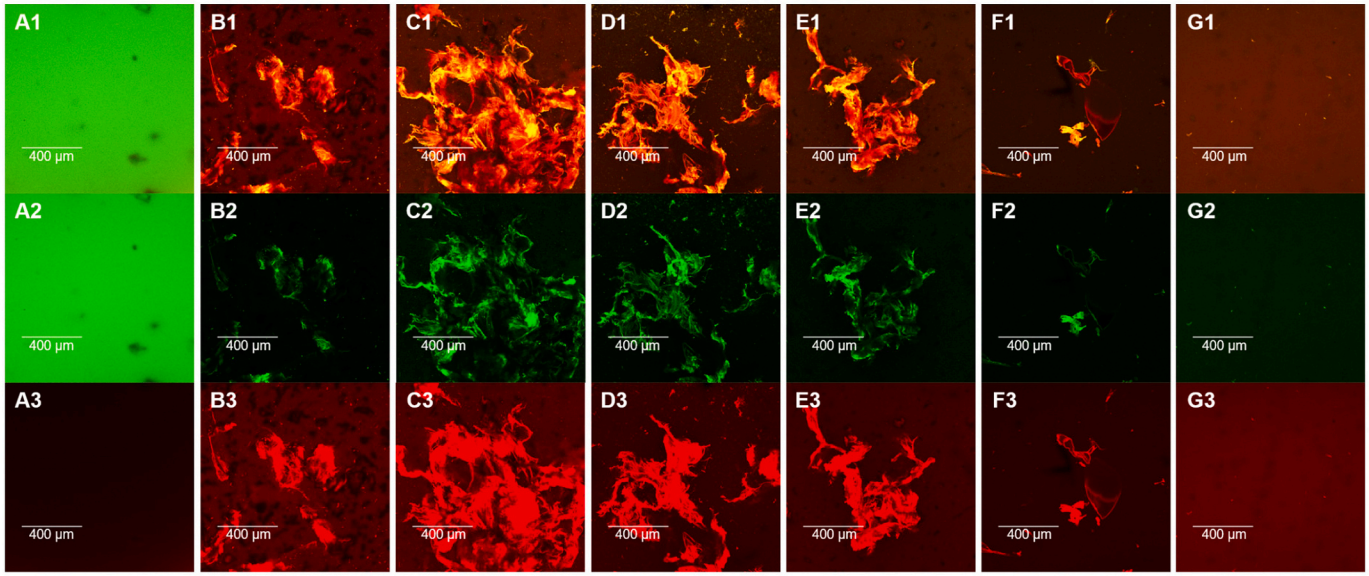

Fig. 3. CLSM images of the samples before heating with mixing ratio of OVA: κ-C at 0:100 (A), 90:10 (B), 92:8 (C), 94:6 (D), 96:4 (E), 98:2 (F), 100:0 (G); The images of merge channel (A1-G1); The images of the channel for κ-C (A2-G2); The images of the channel for OVA (A3-G3).

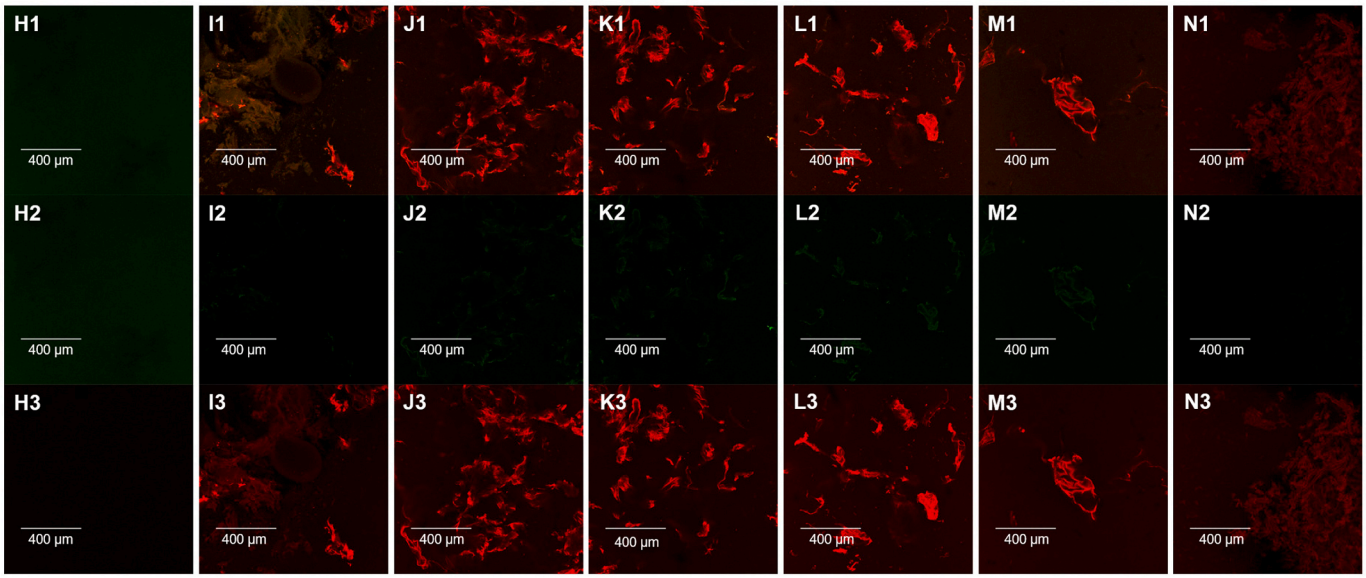

Fig. 4. CLSM images of the samples after heating with mixing ratio of OVA: κ-C at 0:100 (H), 90:10 (I), 92:8 (J), 94:6 (K), 96:4 (L), 98:2 (M), 100:0 (N); The images of merge channel (H1–N1); The images of the channel for κ-C (H2–N2); The images of the channel for OVA (H3–N3).

balanced, the aggregation of the protein related to the better formation of the OVA/κ-C complexes. Meanwhile, the double helix structure of κ-C opens at the warming temperature and then polymerizes during the cooling process. The conformation restoration and spatial rearrangement of the κ-C were exposed more sulphate groups, contributing to the formation of this denser network (Mangione et al., 2003). In the case of 96:4 and 98:2, the OVA/κ-C complexes and the large aggregation of the OVA cannot be observed (Fig. 4L, N). The difficulty in network formation may be induced by the low amount of κ-C. The smaller amount of κ-C can only interact electrostatically with a fraction of the OVA. More of the OVA remains in the aggregated state. In the meantime, the electrostatic repulsion between the OVA/κ-C complexes may inhibit the connection between them. Therefore, except for the κ-C, the samples at mixing ratios of 96:4 and 98:2 had the lowest G^* value at the end of the thermal cycle.

3.5. Schematic analysis of the complex formation in the OVA/κ-C mixtures

Based on the results of zeta potential, turbidity, rheological properties, and CLSM, the schematic model about the effect of κ-C on OVA was proposed in Fig. 5. The OVA solution was uniformly distributed in the pure OVA sample. After adding κ-C, the κ-C interacted with OVA to form the insoluble complexes through the electrostatic force between the NH_3^+ group of the OVA and the OSO_3^- group of the κ-C (Lu et al., 2020). As the κ-C increased, the size of the complexes increased due to the net charge of the system tended to be neutral. When the ratio reached 92:8, the charge of the system reached a balance condition. The zeta potential values were close to 0 and the turbidity touched the highest values (Fig. 1). Some of the OVA molecules were buried in the OVA/κ-C network, forming large but loosely aggregates. To further increase the

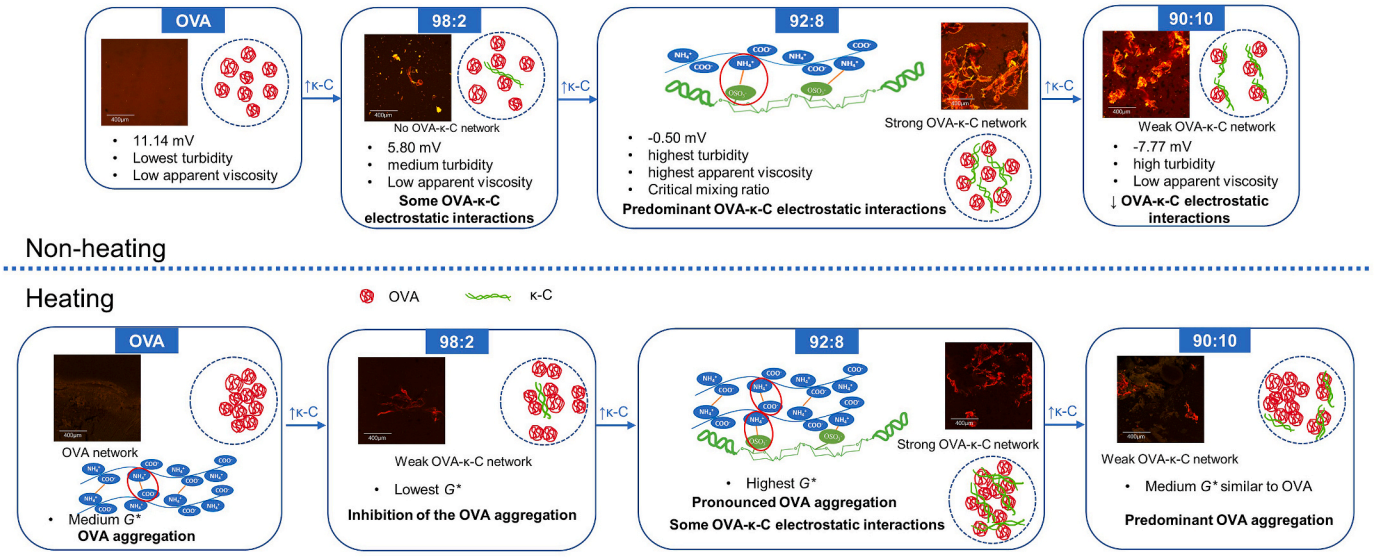

Fig. 5. Schematic model demonstrating the effect of κ-C on the OVA.

ratio of κ-C, the system became negatively charged and the aggregation was inhibited by the electrostatic repulsion. Heating treatment could lead to protein denaturation and the aggregations became smaller. The interactions between OVA and κ-C influenced the thermal gelling process of the mixtures. During the whole gelation period, the mixture at the critical ratio 92:8 always had the highest G^* values (Fig. 2). Overall, the addition of κ-C disturbed the aggregation of protein and formed new electrostatic interactions with the protein. While during the heat process, the OVA/κ-C complexes might partially be destroyed.

3.6. Validation of the proposed model

To verify the proposed schematic model, FTIR analysis was adopted to confirm the structural change of the OVA/κ-C system. The spectra of samples in the region of 960–800 cm^{-1} and 1700-1600 cm^{-1} (amide I) are presented in Fig. 6. Two strong bands at about 927 cm^{-1} and 846 cm^{-1} were observed in κ-C sample. These two bands are considered as the characteristic bands for 3,6-anhydro-D-galactose and D-galactose-4-sulphate, respectively (Gómez-Ordóñez & Rupérez, 2011; Huang et al., 2021). However, these two bands were not observed in the OVA/κ-C mixtures, indicating the interaction formed between OVA and κ-C.

As shown in Fig. 6, the amide I (1700–1600 cm^{-1}) has stronger peak intensity and is usually used as the quantitative area for the calculation of protein secondary structures (Seabourn, Chung, Seib, & Mathewson, 2008). The amide I was primarily from the C═O stretching vibration and N–H bonding of the peptide linkages, and it is sensitive to the protein secondary structures (Dong, Meyer, Brown, Manning, & Carpenter, 2000). Thus, it was used to further analyse the changes in the secondary structures of proteins.

To further confirm the changes of OVA structure, the proportion of secondary structures were calculated and demonstrated in Table 2. The

Table 2
The percentage of secondary structures in different OVA/κ-C samples.

Groups OVA: κ-C (w/w)	Secondary structure (%)			
	β-sheet	Random coil	α-helix	β-turn
90:10	6.65 ± 0.01^{a}	56.69 ± 4.06^{b}	12.93 ± 2.75^{a}	23.73 ± 1.30^{c}
92:8	4.82 ± 0.21^{a}	58.35 ± 1.92^{b}	12.97 ± 3.10^{a}	23.85 ± 1.39^{c}
94:6	5.80 ± 0.73^{a}	58.06 ± 3.77^{b}	13.18 ± 4.36^{a}	22.96 ± 0.13^{c}
96:4	5.19 ± 2.45^{a}	56.09 ± 6.70^{b}	13.97 ± 5.00^{a}	24.74 ± 0.74^{c}
98:2	5.95 ± 0.24^{a}	54.50 ± 0.66^{b}	15.16 ± 0.12^{a}	23.99 ± 0.30^{c}
100:0	7.33 ± 0.42^{a}	54.74 ± 0.02^{b}	12.03 ± 0.30^{a}	25.90 ± 0.74^{c}
H90:10	20.82 ± 2.33^{bc}	33.52 ± 3.77^{a}	36.79 ± 1.46^{c}	8.86 ± 0.01^{a}
H92:8	19.71 ± 1.61^{bc}	37.74 ± 2.82^{a}	31.66 ± 1.87^{b}	10.89 ± 0.67^{ab}
H94:6	20.04 ± 0.55^{bc}	37.16 ± 4.09^{a}	32.67 ± 4.46^{bc}	10.13 ± 3.17^{ab}
H96:4	19.19 ± 0.14^{bc}	36.80 ± 0.71^{a}	34.44 ± 0.14^{bc}	9.57 ± 0.44^{ab}
H98:2	22.28 ± 1.45^{c}	37.86 ± 2.74^{a}	27.41 ± 0.12^{b}	12.45 ± 1.42^{b}
H100:0	18.27 ± 2.25^{b}	40.44 ± 4.21^{a}	30.70 ± 2.52^{bc}	10.59 ± 0.55^{ab}

*H90:10, H92:8, H94:6, H96:4, H98:2, H100:0 indicated the heat-treated samples of mixtures at different mixing ratios. Values are expressed as mean ± standard deviation. Values with different letters in the same column differ significantly at $P < 0.05$ (n = 3).

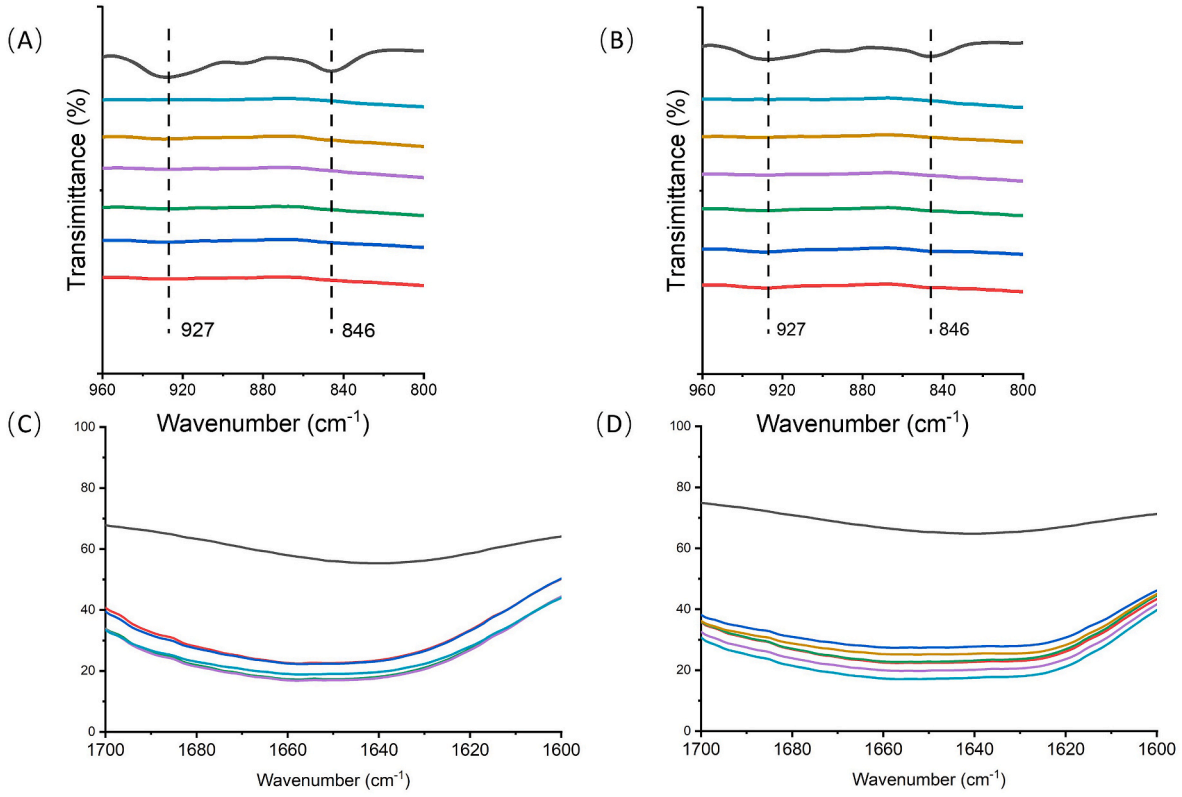

Fig. 6. FTIR spectra of different OVA/κ-C samples. (A) Spectra of the OVA/κ-C mixtures before heating in the region of 960–800 cm-1; (B) Spectra of the OVA/κ-C mixtures after heating in the region of 960–800 cm-1; (C) Spectra of the OVA/κ-C mixtures before heating in the region of amide I; (D) Spectra of the OVA/κ-C mixtures after heating in the region of amide I. OVA: κ-C: black line, 0:100; orange line: 90:10; blue line: 92:8; olive line: 94:6; purple line: 96:4; brown line: 98:2; red line: 100:0. (For interpretation of the references to colour in this figure legend, the reader is referred to the Web version of this article.)

pick was located at 1610–1640, 1640–1650, 1650–1660, and 1660-1700 cm^{-1}, representing β-sheet, random coil, α-helix and β-turn, respectively (Feng, Cai, Wang, Li, & Liu, 2018; Ngarize et al., 2004). The random coil, β-turn, α-helix and β-sheet of OVA were 54.74%, 25.90%, 12.03% and 7.33%. In previous research, the OVA also indicated the same secondary structures, including α-helix (27.9%), β-sheet (29.7%), β-turn (18.2%) and random coil (24.2%) (Sun, Mu, Mohammed, Dong, & Xu, 2020). However, the random coil (54.74%) in this work was the main structure, and it may be because the ordered structure was partially destroyed at low pH. There was no significant difference in the percentage of secondary structures between different mixing ratios samples before heating. It means that the addition of a low concentration of κ-C had not much effect on the OVA secondary structures although they formed OVA/κ-C aggregates.

After heating, the random coil and β-turn of all samples decreased, while the ordered structure α-helix and β-sheet increased. A similar decline of random coil and β-turn was detected when OVA formed conjugates (Geng et al., 2014). The random coil decreased the most from 54.74% to 40.44%, and the β-turn structure also was partial damaged. The ordered α-helix increased to 2 times in the heated OVA, indicating the reorganized of the proteins (Pal et al., 2011). The heat treatment also significantly increased the proportion of the β-sheet. The same trends occurred on β-lactoglobulin gels in heat-induced gelation at low pH (Kavanagh, Clark, & Ross-Murphy, 2000). The rise of the percentage of intermolecular β-sheet related to the interaction between proteins became stronger during the heating phase (Mine, 1995). After adding κ-C, the β-sheet increased but not significantly. The κ-C gelation process in solution has the random coil-to-helix transition which might enhance the formation of β-sheet (Ngarize et al., 2004). However, the effect of mixing ratio on the percentage of the β-sheet after heating cannot be observed. The result of other structures indicated that the addition of low concentration of κ-C had no significant effect on the heating gelation of the OVA.

4. Conclusions

This study aimed to investigate the effects of kappa-carrageenan (κ-C) on the interaction, structure, and rheological properties of ovalbumin (OVA) before and after heating. The zeta potential and turbidity proved that the electrostatic interaction occurred between OVA and κ-C, and the minimum net charge (-0.5 ± 0.3 mV) and maximum turbidity (0.122 ± 0.001 cm^{-1}) were observed at the critical ratio of OVA: κ-C (w/w) at 92:8. Meanwhile, the mixtures at the same ratio had the highest apparent viscosity and the complex modulus (G^*) remained maximum during the thermal cycle. The CLSM showed that the largest insoluble complex existed at 92:8 which was consistent with the results of zeta potential and turbidity. A schematic model was proposed to explain the effects of the critical mixing ratio and heating process on the interaction between OVA and κ-C. The results of FTIR confirmed the interaction between OVA and κ-C and showed that heat treatment significantly increased the ratio of β-sheet in the samples. The strongest combination in OVA/κ-C mixtures enhanced the β-sheet formation. This study aids our knowledge about the interaction of OVA and κ-C and has great potential to develop novel food products containing OVA and κ-C.

CRediT authorship contribution statement

Yuzhu Mao: Conceptualization, Methodology, Investigation, Software, Visualization, Writing – original draft, Writing – review & editing. **Min Huang:** Methodology, Investigation, Software. **Jiapei Bi:** Methodology, Software, Visualization. **Duowen Sun:** Methodology, Investigation, Validation. **Hongliang Li:** Conceptualization. **Hongshun Yang:** Conceptualization, Funding acquisition, Project administration, Supervision, Writing – review & editing.

Declaration of competing interest

There are none to declare.

Data availability

Data will be made available on request.

Acknowledgements

This work was funded by Singapore NRF Industry IHL Partnership Grant (R-143-000-653-281), student support (R-160-002-653-281), Singapore Ministry of Education Academic Research Fund Tier 1 (A-8000469-00-00) and an industry project from Guangzhou Welbon Biological Technology Co., Ltd (R-2017-H-002).

Appendix

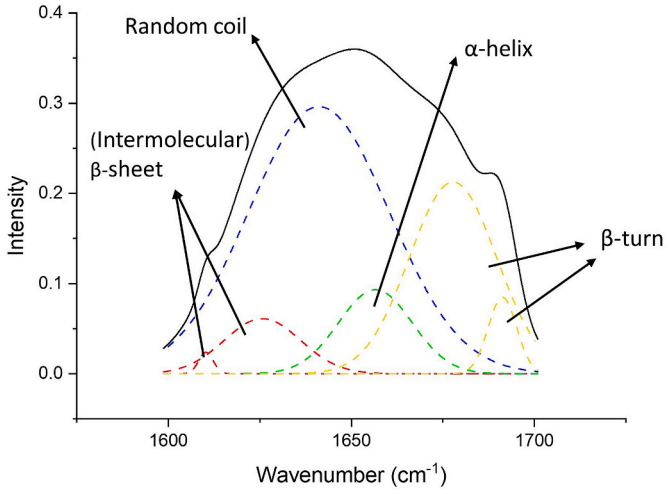

Fig. S1. Curve fitting in deconvoluted FTIR spectra of amide I (solid line: deconvoluted curve; dashed lines: fitted peaks).

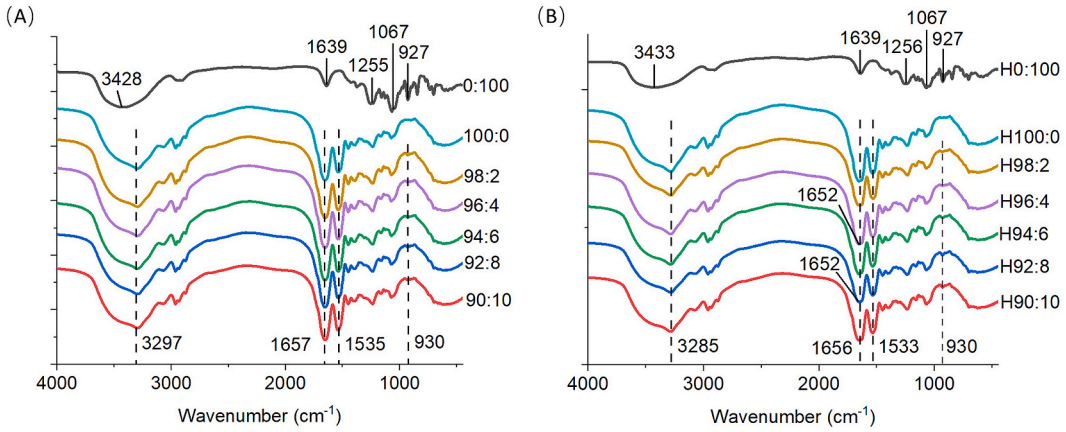

Fig. S2. Fourier transform infrared (FTIR) spectra of different OVA/κ-C samples. (A) Spectra of the OVA/κ-C mixtures before heating; (B) Spectra of the OVA/κ-C mixtures after heating. OVA: κ-C: black line, 0:100; orange line: 90:10; blue line: 92:8; olive line: 94:6; purple line: 96:4; brown line: 98:2; red line: 100:0.

References

Abeyrathne, E., Lee, H., & Ahn, D. U. (2013). Egg white proteins and their potential use in food processing or as nutraceutical and pharmaceutical agents—a review. *Poultry Science, 92*(12), 3292–3299.

Campbell, L., Raikos, V., & Euston, S. R. (2003). Modification of functional properties of egg-white proteins. *Food, 47*(6), 369–376.

Chen, Y., Hu, J., Yi, X., Ding, B., Sun, W., Yan, F., et al. (2018). Interactions and emulsifying properties of ovalbumin with tannic acid. *Lebensmittel-Wissenschaft und -Technologie, 95*, 282–288.

Clark, A., Kavanagh, G., & Ross-Murphy, S. (2001). Globular protein gelation—theory and experiment. *Food Hydrocolloids, 15*(4–6), 383–400.

Determan, A. S., Graham, J. R., Pfeiffer, K. A., & Narasimhan, B. (2006). The role of microsphere fabrication methods on the stability and release kinetics of ovalbumin encapsulated in polyanhydride microspheres. *Journal of Microencapsulation, 23*(8), 832–843.

Dong, A., Meyer, J. D., Brown, J. L., Manning, M. C., & Carpenter, J. F. (2000). Comparative Fourier transform infrared and circular dichroism spectroscopic analysis of α1-proteinase inhibitor and ovalbumin in aqueous solution. *Archives of Biochemistry and Biophysics, 383*(1), 148–155.

Du, L., Brenner, T., Xie, J., & Matsukawa, S. (2016). A study on phase separation behavior in kappa/iota carrageenan mixtures by micro DSC, rheological measurements and simulating water and cations migration between phases. *Food Hydrocolloids, 55*, 81–88.

Feng, J., Cai, H., Wang, H., Li, C., & Liu, S. (2018). Improved oxidative stability of fish oil emulsion by grafted ovalbumin-catechin conjugates. *Food Chemistry, 241*, 60–69.

Geng, X., Cui, B., Li, Y., Jin, W., An, Y., Zhou, B., et al. (2014). Preparation and characterization of ovalbumin and carboxymethyl cellulose conjugates via glycosylation. *Food Hydrocolloids, 37*, 86–92.

Gentile, L. (2020). Protein–polysaccharide interactions and aggregates in food formulations. *Current Opinion in Colloid & Interface Science, 48*, 18–27.

Gómez-Ordóñez, E., & Rupérez, P. (2011). FTIR-ATR spectroscopy as a tool for polysaccharide identification in edible brown and red seaweeds. *Food Hydrocolloids, 25*, 1514–1520.

Gonzalez-Perez, A., Ruso, J., Prieto, G., & Sarmiento, F. (2004). Physicochemical study of ovalbumin in the presence of sodium dodecyl sulphate in aqueous media. *Colloid and Polymer Science, 282*(4), 351–356.

Huang, M., Mao, Y., Li, H., & Yang, H. (2021). Kappa-carrageenan enhances the gelation and structural changes of egg yolk via electrostatic interactions with yolk protein. *Food Chemistry, 360*, Article 129972.

Kang, D., Ryu, S. R., Park, Y., Czarnik-Matusewicz, B., & Jung, Y. M. (2014). pH-induced structural changes of ovalbumin studied by 2D correlation IR spectroscopy. *Journal of Molecular Structure, 1069*, 299–304.

Kavanagh, G. M., Clark, A. H., & Ross-Murphy, S. B. (2000). Heat-induced gelation of globular proteins: Part 3. Molecular studies on low pH β-lactoglobulin gels. *International Journal of Biological Macromolecules, 28*(1), 41–50.

Kobayashi, M., Kumagai, Y., Yamamoto, Y., Yasui, H., & Kishimura, H. (2020). Identification of a key enzyme for the hydrolysis of β-(1→ 3)-xylosyl linkage in red alga dulse xylooligosaccharide from Bifidobacterium adolescentis. *Marine Drugs, 18*(3), 174.

Lam, M., Paulsen, P., & Corredig, M. (2008). Interactions of soy protein fractions with high-methoxyl pectin. *Journal of Agricultural and Food Chemistry, 56*(12), 4726–4735.

Le, X. T., Rioux, L.-E., & Turgeon, S. L. (2017). Formation and functional properties of protein–polysaccharide electrostatic hydrogels in comparison to protein or polysaccharide hydrogels. *Advances in Colloid and Interface Science, 239*, 127–135.

Liu, J., Chai, J., Zhang, T., Yuan, Y., Saini, R. K., Xu, M., … Shang, X. (2021). Phase behavior, thermodynamic and rheological properties of ovalbumin/dextran sulfate: Effect of biopolymer ratio and salt concentration. *Food Hydrocolloids, 118*, Article 106777.

Liu, H., Maruyama, H., Masuda, T., Honda, A., & Arai, F. (2014). Multi-fluorescent micro-sensor for accurate measurement of pH and temperature variations in micro-environments. *Sensors and Actuators B: Chemical, 203*, 54–62.

Lu, Z., Wang, L., Xie, H., Lei, Q., Fang, W., & Lu, X. (2020). Structural transitions of ovalbumin/κ-carrageenan complexes under the effects of pH and composition. *Chemical Physics, 533*, Article 110733.

Mangione, M. R., Giacomazza, D., Bulone, D., Martorana, V., & San Biagio, P. L. (2003). Thermoreversible gelation of κ-Carrageenan: Relation between conformational transition and aggregation. *Biophysical Chemistry, 104*, 95–105.

Mine, Y. (1995). Recent advances in the understanding of egg white protein functionality. *Trends in Food Science & Technology, 6*, 225–232.

Necas, J., & Bartosikova, L. (2013). Carrageenan: A review. *Veterinarni Medicina, 58*(4), 187–205.

Ngarize, S., Herman, H., Adams, A., & Howell, N. (2004). Comparison of changes in the secondary structure of unheated, heated, and high-pressure-treated β-lactoglobulin and ovalbumin proteins using Fourier transform Raman spectroscopy and self-deconvolution. *Journal of Agricultural and Food Chemistry, 52*(21), 6470–6477.

Niu, F., Kou, M., Fan, J., Pan, W., Feng, Z.-J., Su, Y., et al. (2018). Structural characteristics and rheological properties of ovalbumin-gum Arabic complex coacervates. *Food Chemistry, 260*, 1–6.

Niu, F., Niu, D., Zhang, H., Chang, C., Gu, L., Su, Y., et al. (2016). Ovalbumin/gum Arabic-stabilized emulsion: Rheology, emulsion characteristics, and Raman spectroscopic study. *Food Hydrocolloids, 52*, 607–614.

Njintang, N. Y., Parker, M. L., Moates, G. K., Mbofung, C. M., Smith, A. C., & Waldron, K. W. (2006). Rheology and microstructure of achu, a food based on taro (Colocasia esculenta L. Schott), as affected by method of preparation. *Journal of the Science of Food and Agriculture, 86*(6), 902–907.

Sánchez-Gimeno, A. C., Vercet, A., & López-Buesa, P. (2006). Studies of ovalbumin gelation in the presence of carrageenans and after manothermosonication treatments. *Innovative Food Science & Emerging Technologies, 7*(4), 270–274.

Schmitt, C., & Turgeon, S. L. (2011). Protein/polysaccharide complexes and coacervates in food systems. *Advances in Colloid and Interface Science, 167*(1–2), 63–70.

Seabourn, B. W., Chung, O. K., Seib, P. A., & Mathewson, P. R. (2008). Determination of secondary structural changes in gluten proteins during mixing using fourier transform horizontal attenuated total reflectance spectroscopy. *Journal of Agricultural and Food Chemistry, 56*(11), 4236–4243. https://doi.org/10.1021/jf703569b

Souza, C. J., & Garcia-Rojas, E. E. (2017). Interpolymeric complexing between egg white proteins and xanthan gum: Effect of salt and protein/polysaccharide ratio. *Food Hydrocolloids, 66*, 268–275.

Sow, L. C., Chong, J. M. N., Liao, Q. X., & Yang, H. (2018). Effects of κ-carrageenan on the structure and rheological properties of fish gelatin. *Journal of Food Engineering, 239*, 92–103.

Sow, L. C., Toh, N. Z. Y., Wong, C. W., & Yang, H. (2019). Combination of sodium alginate with tilapia fish gelatin for improved texture properties and nanostructure modification. *Food Hydrocolloids, 94*, 459–467.

Spagnuolo, P. A., Dalgleish, D., Goff, H., & Morris, E. (2005). Kappa-carrageenan interactions in systems containing casein micelles and polysaccharide stabilizers. *Food Hydrocolloids, 19*(3), 371–377.

Sun, J., Mu, Y., Mohammed, O., Dong, S., & Xu, B. (2020). Effects of single-mode microwave heating and dextran conjugation on the structure and functionality of ovalbumin–dextran conjugates. *Food Research International, 137*, Article 109468.

Takemasa, M., Chiba, A., & Date, M. (2001). Gelation mechanism of κ-and ι-carrageenan investigated by correlation between the strain– optical coefficient and the dynamic shear modulus. *Macromolecules, 34*(21), 7427–7434.

Tan, J., & Joyner, H. S. (2018). Characterizing wear behaviors of κ-carrageenan and whey protein gels by numerical modeling. *Journal of Food Engineering, 235*, 98–105.

Walayat, N., Wang, X., Nawaz, A., Zhang, Z., Abdullah, A., Khalifa, I., … Lorenzo, J. M. (2021). Ovalbumin and kappa-carrageenan mixture suppresses the oxidative and structural changes in the myofibrillar proteins of grass carp (Ctenopharyngodon idella) during frozen storage. *Antioxidants, 10*(8), 1186.

Wang, S., Van Dijk, J., Odijk, T., & Smit, J. (2001). Depletion-induced demixing in aqueous Protein– polysaccharide solutions. *Biomacromolecules, 2*(4), 1080–1088.
Wijaya, W., Patel, A. R., Setiowati, A. D., & Van der Meeren, P. (2017). Functional colloids from proteins and polysaccharides for food applications. *Trends in Food Science & Technology, 68*, 56–69.
Xie, H., Xiang, C., Li, Y., Wang, L., Zhang, Y., Song, Z., et al. (2019). Fabrication of ovalbumin/κ-carrageenan complex nanoparticles as a novel carrier for curcumin delivery. *Food Hydrocolloids, 89*, 111–121.
Xiong, Z., & Ma, M. (2017). Enhanced ovalbumin stability at oil-water interface by phosphorylation and identification of phosphorylation site using MALDI-TOF mass spectrometry. *Colloids and Surfaces B: Biointerfaces, 153*, 253–262.
Ye, A. (2008). Complexation between milk proteins and polysaccharides via electrostatic interaction: Principles and applications–a review. *International Journal of Food Science and Technology, 43*(3), 406–415.
Zhao, Y., Chen, Z., Li, J., Xu, M., Shao, Y., & Tu, Y. (2016). Formation mechanism of ovalbumin gel induced by alkali. *Food Hydrocolloids, 61*, 390–398.